Lawrence Berkeley National Laboratory

Title

Design of an Achromatic Superconducting Magnet for a Proton Therapy Gantry

Permalink

Journal

ISSN

Authors

Brouwer, L
Caspi, S
Hafalia, R
et al.

Publication Date

2017

DOI

Design of an Achromatic Superconducting Magnet for a Proton Therapy Gantry

L. Brouwer, S. Caspi, R. Hafalia, A. Hodgkinson, S. Prestemon, D. Robin, and W. Wan

Abstract—**Recent studies have shown that strong, alternating focusing magnets can be used to greatly increase the momentum acceptance of hadron therapy gantries. With the high gradients achievable with superconducting magnets a level of momentum acceptance can be reached which may have significant implications to medical gantries and to the introduction of superconducting technology in this area. The design of such a superconducting magnet system for a proton therapy gantry will be presented. The Canted-Cosine-Theta concept is extended to a curved magnet system generating the desired bending and alternating focusing fields for the achromatic optics. Magnetic, structural, and thermal analysis of this design is presented along with preliminary efforts towards fabrication and assembly of the curved magnet.**

Index Terms—**Accelerator magnets, superconducting gantry magnets, proton therapy, ion beam therapy, canted-cosine-theta.**

I. INTRODUCTION

SUPERCONDUCTING magnets are desirable for particle therapy gantries due to their low weight and ability to produce the complex, combined function fields required for achromatic beam optics. Recently, a new superconducting magnet concept called the Alternating Gradient Canted-Cosine-Theta (AG-CCT) was developed to make use of these advantages. A first design study implementing the AG-CCT concept was completed, achieving twenty-five percent momentum acceptance in a compact gantry for proton therapy [1]. Lawrence Berkeley National Laboratory (LBNL) in collaboration with the Paul Scherrer Institute (PSI) and Varian Medical Systems is now developing a superconducting magnet for a similar system. This project is part of the newly established US Office of High Energy Physics Accelerator Stewardship Program and is aligned with the R&D needs for future state-of-the-art ion beam therapy facilities as concluded by a joint DOE and NIH workshop [2].

Superconducting technology is not new to particle therapy treatment facilities, having been implemented in superconducting medical cyclotrons [3], but is only recently nearing use in a clinical gantry. Superconducting magnets have been designed and built for the carbon ion gantry at NIRS in Chiba, Japan and for a compact proton gantry developed by the US company ProNova [4]–[6]. These first superconducting gantry systems are currently in commissioning [7]. While there are several
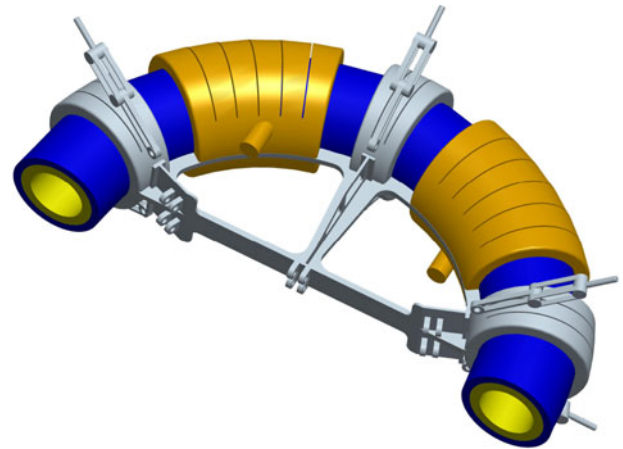
Fig. 1. Gantry magnet cold mass.

additional and different approaches to superconducting gantry magnet design [8]–[11], previous work at LBNL has focused on the use of the Canted-Cosine-Theta (CCT) concept [12]–[14] for the gantry's final bending magnet [15]–[17]. This paper will share the most recent developments of this effort by reporting on the design of a curved AG-CCT superconducting magnet.

The magnet is designed to transport protons of energy 70-220 MeV over the final 135 degrees of bending in a gantry similar to the system presented in [1]. The large momentum acceptance ($\Delta p/p = 20\%$) allows for treatment using a range of energies without magnet field change. With respect to the gantry described in previous work, the number of superconducting magnets has been reduced from three 90 degree bends to this single 135 degree bend, and the location of the scanning magnet system has been moved downstream. In the updated gantry layout a single resistive magnet is included at the start of the gantry which bends the beam upwards by 45 degrees to the superconducting magnet.

II. MAGNET DESIGN

A. Method for Integrating Coil Design With Beam Optics

A process has been developed to closely couple the magnet coil design to the desired beam optics [1]. This begins with the completion of an initial gantry optics design using the simulation code COSY Infinity [18]. An idealized magnetic field description called the sharp-cut-off fringe field (SCOFF) model is used for fast iteration of the optics calculations. The completed SCOFF model design defines an initial magnet geometry and desired integrated multipole content.

A set of conductor windings is then generated based on the SCOFF model geometry and desired fields. The COSY
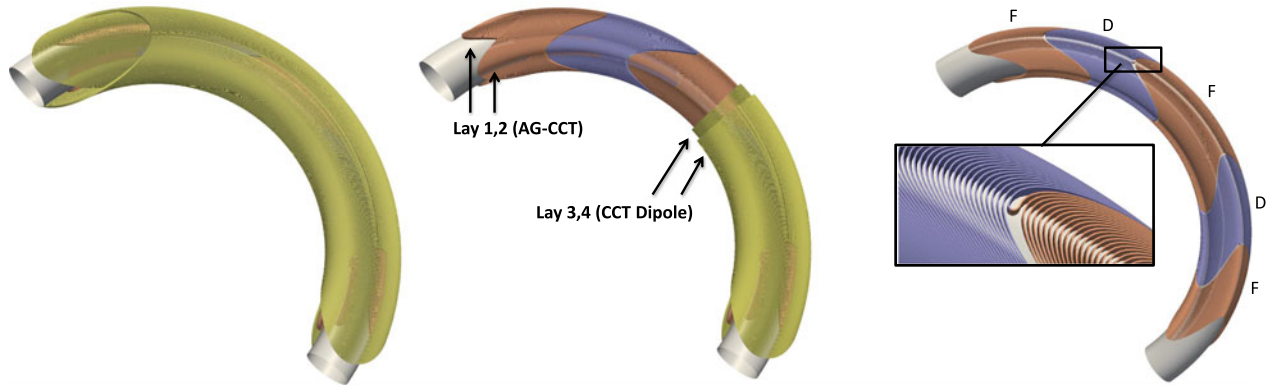
Fig. 2. (Left) four conductor layers, with the dipole cut back to show (center) the inner pair of AG-CCT layers, and the current reversal between a focusing (F) and defocusing (D) section of (right) a AG-CCT layer.

TABLE I
OVERVIEW OF MAGNET PARAMETERS

|	
Bending Radius	900 mm
Bore Radius	105 mm
Magnetic Bend	135 deg
Momentum Acceptance ($\Delta p/p$)	20%
Constant Dipole	2.3 T
Alternating Quadrupole	±22.7 T/m
Stored Energy	0.86 MJ

Fig. 3. Dipole and alternating quadrupole fields generated by the windings are compared to the desired fields from the SCOFF model. The integrated coil fields are seen approaching the zero fringe field SCOFF model.

simulation is then updated such that the magnetic field is no longer generated from a SCOFF model but rather from the geometry of these windings. Since there is no iron present, a simple Biot-Savart integration of the current density over the winding path is used. The flexibility of COSY is such that the coil current and sectioning of the alternating quadrupole windings can be optimized concurrently with the beam optics. This allows for a design which, by generating the field from the windings themselves, includes all magnet curvature and end effects. This has proven to be a preferred method, as it directly couples coil design to desired beam behavior without the need for parametric field description or the transfer of field maps.

B. Four Layer Magnetic Design

The coil and optics design process described in Section II-A was completed using the CCT geometry for the windings. The CCT approach consists of multiple tilted conductor layers, usually in pairs, which are designed and powered such that their transverse fields sum and longitudinal fields cancel. This concept has been shown to be an effective method for producing single harmonic or combined function fields of accelerator quality in both straight and curved magnets [13]–[15], [19]–[22].

The resulting magnetic design consists of the two pairs of curved CCT layers seen in Fig. 2. The innermost pair produces quadrupole fields which alternate along the length of the bend, and the outer pair generates a dipole field which is constant along the length. Table I gives an overview of the geometry and field strengths, Fig. 3 compares the dipole and quadrupole field calculated from the coil design to the SCOFF model, and Fig. 4 shows the vertical field in the magnet's bending plane.

The innermost layers are designed with AG-CCT windings. This is a new concept, described in detail in [1], in which
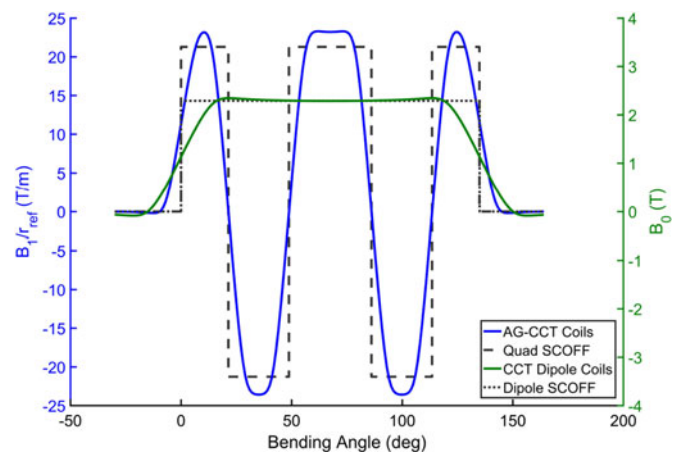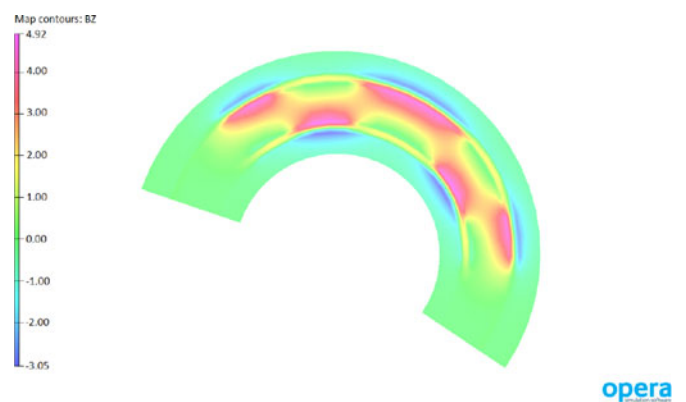
Fig. 4. Vertical field in the bending plane is shown along the length of the magnet in units of Telsa. The interaction of the quadrupole and dipole fields (adding on one side of the bore and subtracting on the other) follows the alternation of the five section AG-CCT layers.

multiple CCT quadrupole winding sections are placed along the length of a bend such that the effective current is reversed between them. The alternation of the field along the length can be tuned by choosing the number and location of transitions between sections. Fig. 2 illustrates the AG-CCT concept and

TABLE II
BASELINE NB-TI WIRE

Bare Dimensions	1.6×1.6 mm
Insulated Dimensions	1.7×1.7 mm
Insulation	Formvar
Cu:SC	2.8:1
Filament Diameter	$20\ \mu$m
Filament Twist Pitch	65 mm
RRR	120
Ic (5 T, 4.2 K)	1570 A

TABLE III
SHORT-SAMPLE MARGIN AT 4.2 K

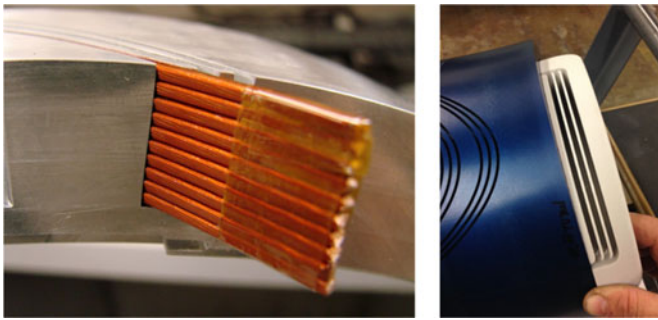| Lay	Type	I/Wire	Wires	B_{cond}	I_c Mar.	Temp. Mar.
1	AG-CCT	763 A	8	5.2 T	29%	1.25 K
2	AG-CCT	763 A	8	5.2 T	29%	1.25 K
3	CCT dipole	922 A	6	4.7 T	29%	1.25 K
4	CCT dipole	922 A	6	3.8 T	45%	1.70 K

Fig. 5. Test demonstrating the winding of a stack of ten insulated square wires into (left) a rectangular channel and (right) a layer-to-layer splice box.

shows the short current reversal which ties the sections together into a continuous coil.

C. Conductor and Short-Sample

The magnet is designed for compatibility with a dry, cryocooler based cooling scheme. In a such a system it is desirable to limit the magnet current and therefore the heat load into the cryostat from the leads. For this reason monolithic wire was chosen as the baseline conductor instead of a high current Rutherford cable (see wire parameters in Table II). Superconducting materials other than Nb-Ti, such as Nb_3Sn and HTS, were considered for their increased current carrying capability and temperature margin, but were ruled out due to cost and difficulties associated with magnet fabrication (such as conductor heat treatments or the winding of tapes). This may be reconsidered after a detailed study of the thermal margins when the cooling scheme is further developed.

The use of single wires as opposed to a Rutherford cable requires a more complicated winding and splicing scheme. The baseline approach is to use a stack of individually insulated wires wound into the rectangular channels of a winding mandrel (see Fig. 5). The wires are connected in series such that for each pair of CCT layers the current flows down first and back through the second. On the return side of each pair of layers all wires are jointed in series (see a slice box prototype in Fig. 5) and on the lead side all but a lead out and in are jointed. A total of 26 joints are needed for the number of wires per layer in Table III. Tests of this winding and splicing approach will be carried out using the two layer practice coil described in Section VII.

The conductor cross section was chosen to use the minimum number of wires in the stack while keeping the current below 1000 A and maintaining a short-sample current margin of near 30% at 4.2 K. The dipole and quadrupole layer pairs are powered

independently and a different number of wires is used in each. Table III shows the number of wires in each set of layers and the peak field at the conductor calculated using the commercial software Opera3D. At a reference temperature of 4.2 K, the resulting current margin of 29% and temperature margin of 1.25 K is the same for both the quadrupole and dipole pairs.

D. Magnet Structure

A key component in the CCT design is the winding mandrel (sometimes called a former) into which the conductor is placed. A mandrel is produced for each layer by machining channels into a curved metallic cylinder. The channels allow for precise placement of the conductor (optimized for the desired field) and the mandrel provides mechanical support against the Lorentz forces. The use of mandrels as structural support internal to the coil pack has been studied in detail for both gantry magnets and high-field dipoles [17], [23].

In addition to the winding mandrels, an external support structure outside of the coil pack is being considered with a preliminary concept shown Fig. 1. A backbone is connected to three mechanical pads to provide additional stiffing, and two cooling pads are located between the mechanical pads for the connection of cryocoolers. The supports which suspend the cold mass within the cryostat are attached to the mechanical pads and the backbone of the structure (not all supports are shown in Fig. 1). Initial mechanical and thermal analysis of the coil pack coupled to this external structure will be described in Sections IV and VI.

III. SINGLE MESH APPROACH TO ANSYS MODELING

An integrated approach was developed in ANSYS to perform magnetic, mechanical, and thermal modeling using a single shared mesh. A solid, meshed model of the conductor, mandrels, external structure, and bounding air box needed for magnetic boundary conditions is generated (see Fig. 6). This mesh is then shared by the models described in Table IV.

The change from one physics model to another is accomplished by: (1) retaining the required regions of the full mesh, (2) changing element type, (3) applying new boundary and contact conditions, and (4) transferring the appropriate loads from previous solutions. The use of the same mesh for all cases allows for simplified load transfer from one model to another using the LDREAD command. The combination of a large mesh and transient analysis made the solution of these models beyond the capability of a desktop computer. Reasonable solution times of less than a day for all cases were obtained on a linux cluster using the HPC ANSYS license and up to twenty cores.

Fig. 6. Full ANSYS model with four layers and an external structure is shown on the left (the additional surrounding air needed for the magnetic model is not included). The central and right-hand figures respectively show a quadrupole and dipole conductor layer extracted from the full model (with their laminated spars underneath).

TABLE IV
INTEGRATED ANSYS MODELING

Type	Element	DOF	Load Transfer
1. Static Mag.	SOLID97	$\vec{A}$	
2. Static Mech.	SOLID185	$\vec{u}$	Lorentz force from 1.
3. Trans. Mag.	SOLID97	$\vec{A}$, VOLT	
4. Trans. Therm.	SOLID70	TEMP	Eddy heating from 3.

IV. MECHANICAL ANALYSIS

A three load step mechanical analysis of the coil pack and external structure was performed using ANSYS. The load steps are: (1) pre-tensioning of the supports which suspend the cold mass within the cryostat , (2) cooldown to 4.2 K, and (3) powering of the magnet to peak operating current. The Lorentz force loads for the final step were transferred from a previously solved magnetic model in ANSYS (see Table IV). These forces were compared on an element by element basis with an Opera3D model and found to be within 5% of each other.

A baseline material of copper was used for the cooling pads and aluminum for the mandrels and external structure. Anisotropic material properties for the conductor channel were determined using the rule of mixtures for a stack of Nb-Ti wires impregnated with epoxy [24]. The von Mises stress in a central cross section after the final load step (peak current operation) can be seen in Fig. 7, and the net displacement of the cold mass in Fig. 8. For all load steps the von Mises stress remains below 55 MPa and the displacement below 0.29 mm.

V. AC LOSSES

The momentum acceptance of a gantry magnet is closely coupled to the field ramping rate required during treatment. For example, estimates have shown a change in momentum acceptance from 8% to the 20% can lower the required peak dipole ramp rate by a factor of ten. Because the magnet heat load scales with the ramp rate (and in some cases the square of the rate), a large momentum acceptance is beneficial for the thermal design.
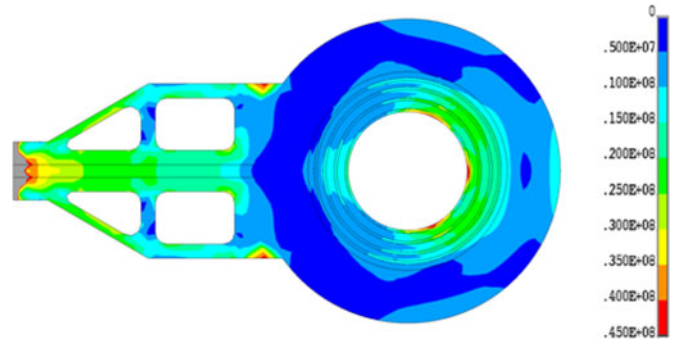

Fig. 7. Von Mises stress is shown in a central cross section of the geometry. The peak stress is 55 MPa in the external structure and 45 MPa in the coil pack.
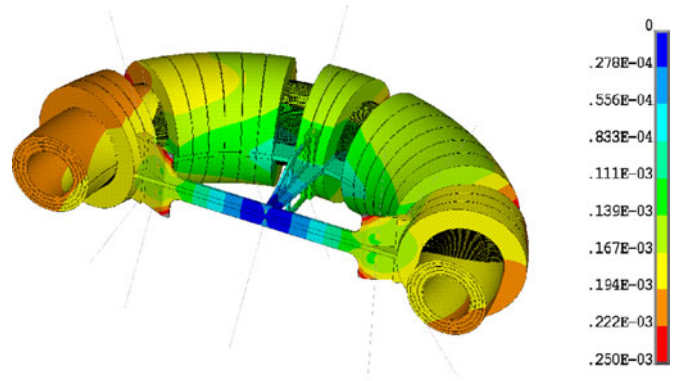

Fig. 8. Net displacement resulting from the Lorentz force is shown for the final load step. The peak displacement is 0.29 mm in the external structure and 0.22 mm in the coil pack.

Two sources of AC losses have been considered: (1) eddy current loss in the structural materials, and (2) AC loss in the conductor. The initial studies in this paper will focus on a peak dipole ramp rate of 0.02 T/s which corresponds to estimates for a 20% momentum acceptance. More detailed studies are in progress to investigate the losses during a typical treatment including periods of lower ramp rate and resting (during which the magnet temperature can recover). The resulting cold mass tem-
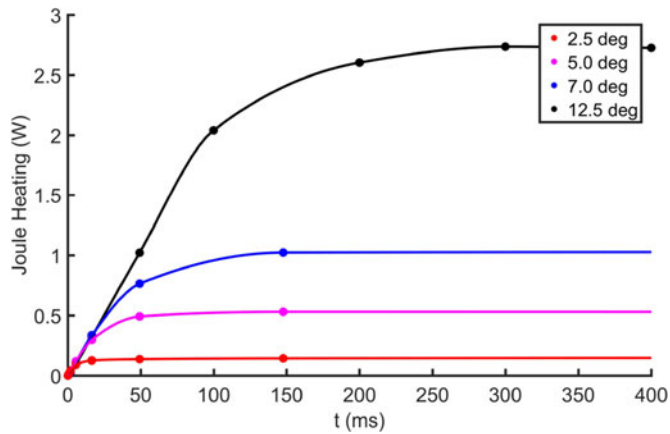
Fig. 9. Total eddy current loss in all four mandrels as a function of time from the start of the ramp. The results are shown for a constant dipole ramp rate of 0.02 T/s and lamination widths from 2.5 to 12.5 degrees of bend angle.

peratures and net cryogenic load for a treatment duty cycle will determine if modifications to the baseline design are necessary.

A. Eddy Current Losses in the Structure

The eddy current losses in the magnet structure were simulated using the transient magnetic ANSYS model described in Table IV. A laminated approach to constructing the winding mandrels and external structure was studied. Results showing the net power deposited in the mandrels for several different lamination bend angles can be seen in Fig. 9. From this study a baseline mandrel lamination width of six degrees was selected, making the total loss 0.7 W for a dipole ramp rate of 0.02 T/s. An investigation of the eddy currents in the preliminary external structure using the same ANSYS model is in progress, with material selection and lamination schemes being considered to bring the losses to an acceptable level.

B. AC Losses in the Conductor

A method was developed to estimate the AC loss in the conductor using a combination of the ANSYS mesh, Opera3D, and analytic loss approximations. First the location and current direction of each conductor element is exported from the ANSYS mesh. Then the magnetic field transverse to the current direction at each of these locations is calculated using Opera3D. With this information, analytic formulas for the hysteresis, inter-filament coupling current (IFCC), and stabilizer loss [25], [26] can be used to estimate the heating within each ANSYS mesh element. This method was applied to estimate the losses assuming the baseline conductor properties in Table II and a dipole ramp rate of 0.02 T/s. The results of this study showed a net hysteresis loss of 3.0 W, IFCC loss of 1.3 W, and stabilizer loss of 1.0 W.

VI. Thermal Analysis

The use of the ANSYS mesh for the eddy current and conductor loss calculations allows for simplified load transfer to the thermal model described in Table IV. A study was performed to find the temperature distribution due to a fixed dipole ramp rate of 0.02 T/s. An initial temperature of 4.2 K was set for all nodes
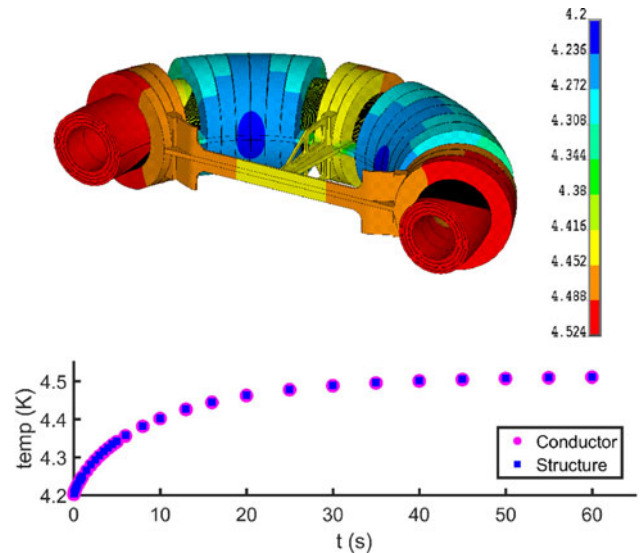

Fig. 10. Steady-state temperature distribution in the cold mass (top) and peak temperature as a function of time (bot) for a 0.02 T/s dipole ramp.

and the joule heating from eddy current and AC loss models were applied to the mandrel and conductor elements. Patches of nodes on the cooling pads at the cryocooler locations were fixed at 4.2 K, and the contact conditions radially between cold mass layers were estimated using the assembly gap and epoxy properties.

Fig. 10 shows the peak temperature as a function of time into the ramp and the final, steady state temperature distribution in the cold mass. After ramping for 60 seconds, the peak temperature in the cold mass rises to a value 320 mK above the starting temperature of 4.2 K. The peak temperatures are located in the magnet ends which is away from the peak field on the conductor. When the distribution of the field on the conductor is considered, the temperature rise due to the conductor and mandrel eddy current losses reduces the thermal margin from the 1.25 K given in Table III to 1.1 K. This is within the initial design requirement of a 1.0 K temperature margin, which is planned to be further refined following the test of a prototype magnet.

VII. Thirty Degrees Practice Coil

Thirty degrees of the two quadrupole layer mandrels was fabricated using the baseline lamination size of six degrees. These ten laminations can be seen in Fig. 11. Channels were machined into the parts to form three sections of the AG-CCT, resulting in two current reversals per layer. A small number of turns per section (five) was chosen to minimize the overall bend angle of the assembly while still allowing for realistic winding tests of full turns and current reversal transitions.

A thermal dovetail was machined into the axial faces of the laminations so adjacent pieces could be assembled together using thermal shrinkage of one part at liquid nitrogen temperature (see Fig. 12). A single dowel pin and slot was included to "clock" the azimuthal alignment of the laminations so the bend of the torus and the machined channels are matched during assembly.
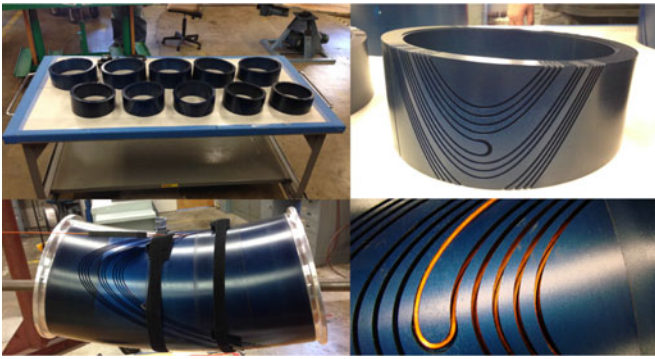
Fig. 11. Curved laminations for the two layer, (top) 30 degrees bend practice coil and (bot) the assembled inner layer being wound.
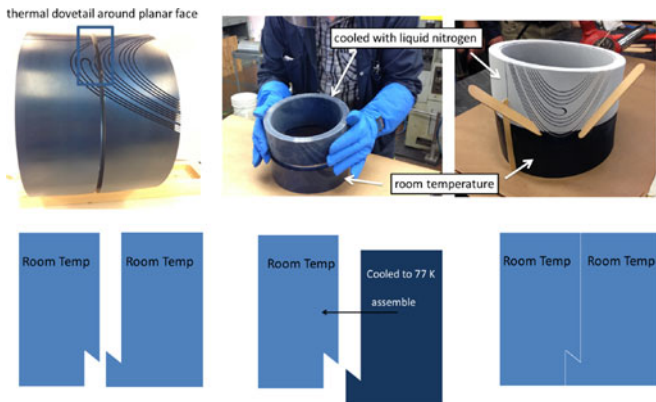

Fig. 12. Assembly of adjacent laminations using a thermal dovetail and liquid nitrogen for cooling.

The laminations for both layers have been assembled, and the winding is in progress.

The mandrels will follow the assembly and epoxy impregnation steps anticipated for the final magnet. The proposed layer-to-layer assembly method is similar to the process used at LBNL for straight CCT magnets. G10 sheets are used to shim the gap between layers and a mechanical puller asissts to assemble one layer inside another. After this assembly the layers will be impregnated together using an external potting tooling or vacuum bag approach.

VIII. CONCLUSION

The design of an achromatic gantry magnet for a proton therapy gantry was presented. Four layers of conductor based on the CCT and AG-CCT concept is used to produce the desired constant dipole and alternating quadrupole fields. A method for integrating magnetic, mechanical, and thermal analysis in ANSYS was developed and applied to model the coil pack coupled to an external structure. Finally, efforts towards magnet fabrication and assembly were shown for a two layer practice coil.

REFERENCES

[1] W. Wan *et al.*, "Alternating-gradient canted cosine theta superconducting magnets for future compact proton gantries," *Phys. Rev. Special Topics, Accel. Beams*, vol. 18, no. 10, 2015, Art. no. 103501.

[2] Workshop on ion beam therapy summary report (2013). [Online]. Available: http://science.energy.gov/~/media/hep/pdf/accelerator-rd-stewardship/Workshop_on_Ion_Beam_Therapy_Report_Final_R1.pdf

[3] J. Alonso and T. Antaya, "Superconductivity in medicine," *Rev. Accelerators Sci. Tech.*, vol. 5, pp. 227–263, 2012.

[4] Y. Iwata, K. Noda, T. Shirai, T. Murakami, and T. Furukawa, "Design of a superconducting rotating gantry for heavy-ion therapy," *Phys. Rev. Special Topics, Accel. Beams*, vol. 15, no. 4, 2012, Art. no. 044701.

[5] Y. Iwata, K. Noda, T. Shirai, T. Furukawa, and T. Murakami, "Development of curved combined-function superconducting magnets for a heavy-ion rotating-gantry," *IEEE Trans. Appl. Supercond.*, vol. 23, no. 3, 2014, Art. no. 4400505.

[6] V. Derenchuk, "The ProNova SC360 Gantry," Modern Hadron Therapy Gantry Developments, Cockcroft Inst., Daresbury, U.K., Tech. Rep., Jan. 2014.

[7] Y. Iwata *et al.*, "Beam commissioning of a superconducting rotating-gantry for carbon-ion radiotherapy," *Nuclear Instrum. Methods Phys. Res. A*, vol. 834, pp. 71–80, 2016.

[8] C. Priano, P. Fabbricatore, S. Farinon, R. Musenich, M. Perrella, and S. Squarcia, "A superconducting magnet for a beam delivery system for carbon ion cancer therapy," *IEEE Trans. Appl. Supercond.*, vol. 12, no. 1, pp. 988–992, Mar. 2002.

[9] D. Trbojevic, R. Gupta, E. Keil, B. Parker, and A. Sessler, "Superconducting non-scaling FFAG gantry for carbon/proton cancer therapy," in *Proc. 2007 IEEE Particle Accelerator Conf.*, 2007, Art. no. THPMS092.

[10] A. Gerbershagen, D. Meer, J. Schippers, and M. Seidel, "A novel beam optics concept in a particle therapy gantry utilizing the advantages of superconducting magnets," *Zeitschrift fr Medizinische Physik*, vol. 26, no. 3, pp. 224–237, Sep. 2016.

[11] C. Calzolaio *et al.*, "Preliminary magnetic design of a superconducting dipole for future compact scanning gantries for proton therapy," *IEEE Trans. Appl. Supercond.*, vol. 26, no. 3, Apr. 2016, Art. no. 4401005.

[12] D. Meyer and R. Flasck, "A new configuration for a dipole magnet for use in high energy physics applications," *Nuclear Instrum. Method Phys. Res. A*, vol. 80, no. 2, pp. 339–341, 1970.

[13] C. Goodzeit, M. Ball, and R. Meinke, "The double-helix dipole—A novel approach to accelerator magnet design," *IEEE Trans. Appl. Supercond.*, vol. 13, no. 2, pp. 1365–1378, Jun. 2003.

[14] S. Caspi *et al.*, "The Canted-Cosine-Theta magnet (CCT)—A concept for high field accelerator magnets," *IEEE Trans. Appl. Supercond.*, vol. 24, no. 3, Jun. 2014, Art. no. 4001804.

[15] D. Robin *et al.*, "Superconducting toroidal combined-function magnet for a compact ion beam cancer therapy gantry," *Nuclear Instrum. Method Phys. Res. A*, vol. 659, no. 1, pp. 484–493, 2011.

[16] S. Caspi *et al.*, "Conceptual design of a 260 mm bore 5 T superconducting curved dipole magnet for a carbon beam therapy gantry," *IEEE Trans. Appl. Supercond.*, vol. 22, no. 3, Jun. 2012, Art. no. 4401204.

[17] S. Caspi *et al.*, "A superconducting magnet mandrel with minimum symmetry laminations for proton therapy," *Nuclear Instrum. Method Phys. Res. A*, vol. 719, pp. 44–49, 2013.

[18] M. Berz and K. Makino, *Michigan State University Technical Report*, no. MSUHEP-060803, 2006.

[19] A. V. Gavrilin, M. D. Bird, V. E. Keilin, and A. V. Dudarev, "New concepts in transverse field magnet design," *IEEE Trans. Appl. Supercond.*, vol. 13, no. 2, pp. 1213–1216, Jun. 2003.

[20] H. Witte, T. Yokoi, S. Sheehy, and K. Peach, "The advantages and challenges of helical coils for small accelerators—A Case Study," *IEEE Trans. Appl. Supercond.*, vol. 22, no. 2, Apr. 2012, Art. no. 4100110.

[21] S. Farinon and P. Fabbricatore, "Refined modeling of superconducting double helical coils using finite element analyses," *Supercond. Sci. Technol.*, vol. 25, no. 6, 2012, Art. no. 065006.

[22] C. Goodzeit, R. Meinke, and M. Ball, "Combined function magnets using double-helix coils," in *Proc. Int. Conf. Particle Accelerator*, 2007, pp. 560–562.

[23] L. Brouwer, D. Arbelaez, S. Caspi, H. Felice, S. Prestemon, and E. Rochepault, "Structural design and analysis of Canted-Cosine-Theta dipoles," *IEEE Trans. Appl. Supercond.*, vol. 24, no. 3, Jun. 2014, Art. no. 4001506.

[24] K. Chow and G. Millos, "Measurements of modulus of elasticity and thermal contraction of impregnated Niobium-Tin and Niobium-Titanium composites," *IEEE Trans. Appl. Supercond.*, vol. 9, no. 2, pp. 213–215, Jun. 1999.

[25] M. Wilson, *Superconducting Magnets*. London, U.K.: Oxford Univ. Press, 1983.

[26] B. Turck, F. Lefevre, M. Polak, and L. Krempasky, "Coupling losses in rectangular multifilamentary superconducting composite," *Cryogenics*, vol. 22, no. 9, pp. 441–450, 1982.